IEEE Access
Multidisciplinary | Rapid Review | Open Access Journal

Received March 18, 2021, accepted March 28, 2021, date of publication April 1, 2021, date of current version April 9, 2021.

Digital Object Identifier 10.1109/ACCESS.2021.3070355

2-D Analysis Method for Synchronous Reluctance Motors Considering End-Plate Effect

RAE-EUN KIM[1,2], JAE-GIL LEE[2], JUNG-MOO SEO[2], AND SEUNGYONG HAHN[1]
[1]Department of Electrical and Computer Engineering, Seoul National University, Seoul 08826, South Korea
[2]Korea Electronics Technology Institute, Bucheon 14502, South Korea

Corresponding author: Jae-Gil Lee (jaykleee@gmail.com)

This work was supported by the Ministry of Trade, Industry and Energy (MOTIE) and Korea Evaluation Institute of Industrial Technology (KEIT) of the Republic of Korea under Grant 20011368 and Grant 20013372.

ABSTRACT This paper presents a 2-D analysis of synchronous reluctance motors (SynRMs) considering the end-plate effect. In an electric machine with a laminated steel core, an end-plate is often attached to the rotor core to support the structural robustness of the machine. End-plates occasionally comprise carbon-steel, which changes the magnetic behavior of the electric machine. Thus, an electric machine that utilizes the 3-D finite element analysis (FEA) should be designed to consider the comprehensive magnetic flux path. However, the application of 3-D FEA for the whole design process is computationally expensive. Therefore, we proposed a 2-D FEA-based design strategy that can consider the additional magnetic path of the end-plate for SynRMs. The proposed analysis method was developed based on the magnetic equivalent circuit analysis and d- and q-axis flux linkage calculation. The effectiveness of the proposed method was verified by presenting the actual design case of a SynRM and via an experimental study.

INDEX TERMS End-plate, finite element analysis (FEA), magnetic equivalent circuit (MEC), synchronous reluctance motor (SynRM).

I. INTRODUCTION

In the development of electric machines, 2-D finite element analysis (FEA) can be used to analyze the electromagnetic characteristics of the machine owing to its axial symmetry. However, in cases where the axial symmetry is distorted or the behavior of the magnetic field cannot be neglected, such as rotor overhangs, skew structures, and additional peripheral geometries for fabrication, 2-D FEA cannot guarantee sufficient accuracy. In particular, when a highly accurate analysis is required owing to strict performance requirements, analysis errors due to the 2-D technique occasionally cause significant problems. Hence, 3-D FEA that considers the comprehensive magnetic behaviors is utilized to achieve high accuracy.

Meanwhile, the end plate, called a clamping or retaining plate, is used to ensure the structural robustness of the stacked core of an electric machine [1]–[3]. The end-plate is generally a solid structure comprising materials such as stainless steel or carbon-steel. In particular, the end-plate with magnetic materials can potentially alter the magnetic behavior in the electric machine owing to the additional leakage and linkage paths associated with the magnetic materials. Hence, in the absence of axial symmetry, 2-D analysis cannot be used—in other words, 3-D FEA becomes inevitable. However, the application of 3-D FEA for the whole machine design process is computationally expensive, as iterative modeling and analysis are required.

Several studies have been conducted to analyze the 3-D structure of the motor with the objective to reduce time in terms of overhang [4]–[11] and skewing [12]–[16]; however, only a few studies consider the end-plate effect [3], [17]–[18].

In this regard, an analysis to effectively consider the end-plate effect of a synchronous reluctance motor (SynRM) is proposed in this paper. The proposed strategy can be summarized as follows: 1) The d- and q-axis flux linkages are analyzed via 2-D FEA by neglecting the end-plate effect; 2) a q-axis magnetic equivalent circuit (MEC) is constructed based on the geometry of the target machine and end plates; 3) the corresponding coefficient based on the MEC model is derived; 4) the updated flux linkage is calculated using proposed formulas; 5) the target machine is analyzed via 2-D FEA based on the new flux linkage and its angle obtained in 4); 6) the q-axis flux linkage and motor performance are calculated based on the results obtained in 5).

The associate editor coordinating the review of this manuscript and approving it for publication was Atif Iqbal.

TABLE 1. Specifications of SynRM.

Parameter	Unit	Value
Number of phases	-	3
Number of poles	-	4
Number of slots	-	72
Outer diameter	mm	432
Axial length	mm	300
Rated power	kW	75
Rated speed	r/min	1,800
Rated torque	Nm	398

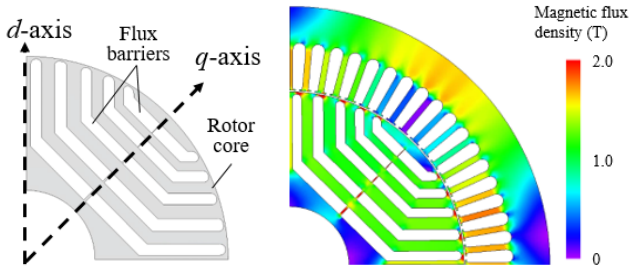

FIGURE 1. 2-D Analysis of SynRM. (a) rotor analysis model with d- and q-axis. (b) Magnetic flux density at rated load condition.

The effectiveness of the proposed method is verified to present the actual design case of the SynRM with the 3-D FEA and experimental results.

The remainder of this paper is organized as follows: The detailed methodology of the proposed method is explained in Section II. The proposed method is validated by presenting the analyzed results from the design application of an actual SynRM, which is discussed in Section III. the conclusions of the study are presented in Section IV.

II. ANALYSIS METHOD CONSIDERING END-PLATE EFFECT

A SynRM is designed with an air region called a magnetic flux barrier in the rotor. This barrier is designed to minimize the leakage of the magnetic flux from the stator; in addition, the barrier generally has three to five layers depending on the size, capacity, and ease of manufacture [19]–[23]. To obtain high-power density, the target SynRM is designed based on a rotor structure of five layers for a large difference between the d- and q-axes reluctances.

First, the industrial four-pole 75 kW class SynRM was designed via 2-D FEA, commonly used in the general design of radial flux machines. The design details of the motor are summarized in Table 1, and the magnetic flux density distribution obtained via 2-D FEA at the rated output power is shown in Fig. 1.

A. ROTOR END-PLATE

Fig. 2 shows a typical rotor assembly of a SynRM comprising a lamination core, a shaft, and an end-plate. The end-plate is

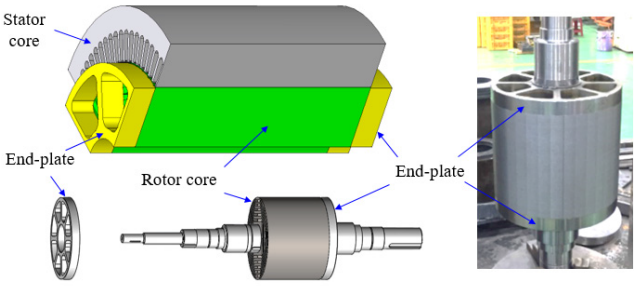

FIGURE 2. Rotor structure of SynRM with end-plates.

TABLE 2. Analysis and test results of SynRM.

Contents	2-D FEA	3-D FEA	Test
Torque (Nm)	398.1	398.9	398.3
Current (A)	187.6	219.6	219.6
Current angle (deg)	66	73	75
Efficiency (%)	97.0	96.0	95.7

crucial for ensuring a tight bonding of the laminated rotor. The structural component occasionally affects the electromagnetic performances of the rotor that comprises magnetic materials such as carbon-steel. Because the structure makes the analysis model lose the axial symmetry, a 3-D analysis becomes inevitable.

The analyses and experimental results of a 75 kW class SynRM with the end plates comprising carbon steel are summarized in Table 2. The 2-D FEA results, wherein the end-plate effect is not considered, exhibits the lowest input current and the highest efficiency at the required torque. However, the results of 3-D FEA and experimental measurements exhibit a remarkable difference from the 2-D analysis results, as summarized in Table 2. Even though 3-D FEA and experiment results corresponded well, the analysis time for a single case exceeded ten hours. Hence, a rapid analysis method that can be applied for the whole design process has been developed in this study.

B. OBSERVATION OF MAGNETIC FLUX BEHAVIOR

Fig. 3(a) shows the distribution of the magnetic flux density of the SynRM at the rated input condition, which is analyzed via 3-D FEA. The flux path in the end-plate was observed to cause distortion in the intended flux and leakage paths. In detail, two analysis models, where the d- and q-axes currents are separately excited, are generated by dividing the rated current and phase angle. Figs. 3(b) and (c) show the magnetic flux behaviors of the end-plate by d- and q- axis respectively.

The magnetic flux caused by the d-axis current passes through the core region of the rotor. However, the magnetic flux caused by the q-axis current crosses the flux barriers which have high reluctance. Therefore, the magnetic flux caused by the q-axis current flows toward the end plate where

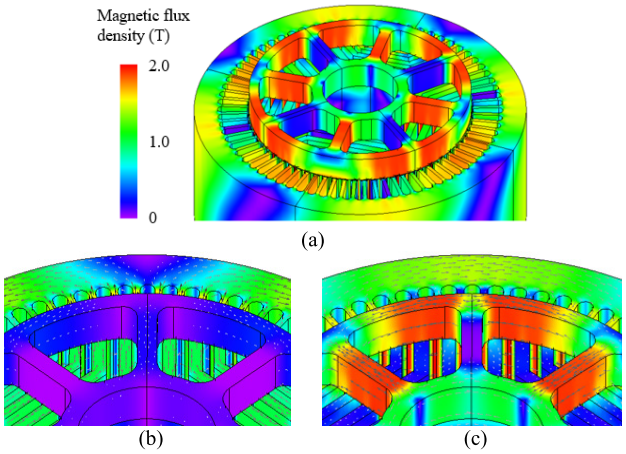

FIGURE 3. 3-D Magnetic flux density of the SynRM end-plate: (a) at rated current. (b) with only d-axis current. (c) with only q-axis current.

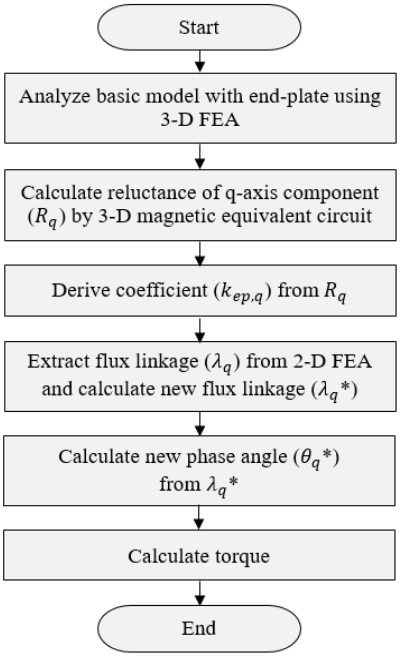

FIGURE 4. Flowchart of the proposed analysis method.

the reluctance is relatively smaller, and the magnetic flux density of the end plate is saturated. Overall, the end-plate significantly affects the q-axis magnetic circuit and reduces the system reluctance by the parallel flux path.

C. PROCEDURE OF THE PROPOSED ANALYSIS METHOD

To rapidly analyze the SynRM considering the end-plate effect, an analysis strategy based on the q-axis MEC and 2-D FEA was developed. The overall procedure of the proposed method is shown in Fig. 4. The detailed description of each step is as follows:

1) 3-D FEA OF BASIC MODEL WITH END PLATE

First, the 3-D FEA of the SynRM basic model reflecting the end-plate is performed. At this time, analyze for a short time step because it is to check the effect of the leakage magnetic flux. Then, the saturation region of the end plate by the q-axis current is analyzed.

2) ANALYZING SynRM BY 2-D FEA

First, the target machine is analyzed via 2-D FEA, neglecting the end-plate effect. This result will be adjusted in the subsequent steps.

3) CONSTRUCTING Q-AXIS MEC

As described in Section II.B, because the end-plate considerably influences the q- axis flux path of SynRM, q-axis MEC is required. In this section, the end-plate effect when applying a q-axis current is analyzed through MEC modeling of the rotor core and end-plate of SynRM.

Fig. 5 (a) schematically shows the q-axis magnetic flux path formed toward the end-plate and rotor core side of generated from the stator when the q-axis current is applied. As shown in Fig. 5 (b), this magnetic flux path can be represented by a parallel system of the reluctance R_{ep}, which passes through the end-plate side and the main magnetic path, R_{main} passing through the rotor core side. Therefore, the change of the q-axis inductance can be estimated according to the presence or absence of the end-plate by calculating the reluctance ratio of R_{main} and R_{ep}.

First, to show the calculation process of R_{main}, the shape of the rotor core and corresponding design parameters are shown in Fig. 6 (a). The rotor core comprises a five-layered air barrier, center-post, and bridge structure to withstand the stress during rotation. The center-post and bridge region are designed to be as thin as possible to minimize leakage flux; thus, they operate close to complete magnetic saturation when the load current is applied. Hence, the center-post and bridge can be treated the same as the air region for constructing the MEC model. The q-axis MEC representing the flux path through the rotor core can be represented as shown in Fig. 6 (b). Here, R_{bi1} and R_{bi2}, which represent the reluctances of the i-th layer, can be calculated by (1)–(2) based on the design parameters expressed in Fig. 6 (a). Finally, the total reluctance R_{main} can be calculated by (3).

$$R_{bi1} = \frac{2t_i}{\mu_0(wi_{i1} + wi_{i2})l_{st}}, \tag{1}$$

$$R_{bi2} = \frac{2t_i}{\mu_0(wo_{i1} + wo_{i2})l_{st}}, \tag{2}$$

$$R_{main} = \frac{2\sum_i R_{bi1} \sum_i R_{bi2}}{\sum_i (R_{bi1} + R_{bi2})}, \tag{3}$$

where the corresponding shape parameters are represented in Fig. 6.

Next, the configuration of Rep representing the magnetic flux path of the end-plate side and the corresponding design parameters are illustrated in Figs. 7 (a) and (b). The magnetic flux path due to the q-axis current bypassing the end-plate can be divided two major reluctance components: R_{qr} and R_{qc}.

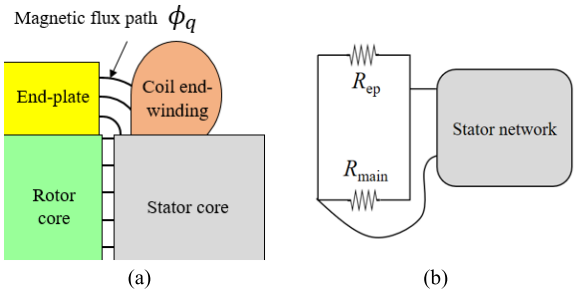

FIGURE 5. Theq-axis MEC modeling of the SynRM: (a) rotor structure and linkage flux path. (b) q-axis MEC.

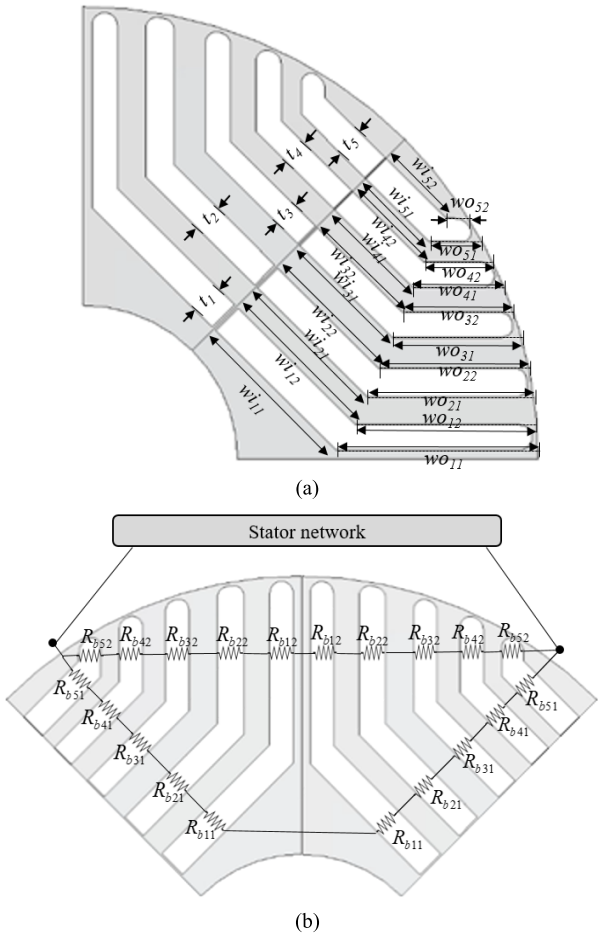

FIGURE 6. q-axis MEC modeling of the rotor core: (a) rotor structure and corresponding design parameters. (b) the q-axis MEC.

The R_{qr} represents the reluctance of radial path through the center rib, and R_{qc} is the reluctance of circumferential path forming through the outer surface of the end-plate. Both reluctances include air regions due to saturation of end-plate, as shown in Fig. 7(c). In this case, assuming all the flux paths are saturated, the permeability of these flux path can be regarded as μ_0. Each of lumped components can be calculated by (4)–(7) based on the geometry.

$$R_{qr,plate} = \frac{w_r}{\mu_0 h d_r}, \tag{4}$$

$$R_{qr,air} = \frac{w_a}{4\mu_0 h(s_1 + s_2)}, \tag{5}$$

$$R_{qc,plate} = \frac{w_c}{\mu_0 h d_c}, \tag{6}$$

$$R_{qc,air} = \frac{s_1 + s_2}{2\mu_0 h w_a}, \tag{7}$$

where the corresponding shape parameters are represented in Fig. 7.

Then, the total reluctance of the end-plate by q-axis current can be calculated by (10).

$$R_{qr} = R_{qr,plate} \parallel R_{qr,air}, \tag{8}$$

$$R_{qc} = R_{qc,plate} \parallel R_{qc,air}, \tag{9}$$

$$R_{ep} = 2(R_{qr} \parallel R_{qc}). \tag{10}$$

4) DERIVING THE CORRECTION COEFFICIENT FROM THE MEC ANALYSIS

Because the end-plate and the laminated core are located in the axial direction, the reluctance is formed in parallel, as shown in Fig. 5. Here, the correction coefficient k_{ep} is derived based on the end-plate reluctance R_{ep} and the reluctance R_{main} of the rotor core, which were previously calculated via the MEC analysis. The magnetic flux generated by the stator current passes through the air gap and is divided by the reluctance ratio of the rotor core and end-plate according to the magnetic flux divider's law. Finally, the correction coefficient k_{ep} is defined as the reluctance ratio by (11) to consider the 3-D effect according to the presence or absence of the end-plate.

$$k_{ep} = \frac{R_{main}}{R_{main} + R_{ep}}. \tag{11}$$

5) CALCULATION THE UPDATED FLUX LINKAGE

The q-axis flux linkage λ_q is updated by (12) and (13) with the flux linkage obtained by the 2-D analysis and the k_{ep}. Then, the magnetic flux phase angle θ_0 is calculated by (14), as illustrated in Fig. 8. Since the updated q-axis flux linkage also affects the total flux amount, a new total flux value is derived by (15) with the d-axis flux linkage λ_d.

$$\Delta\lambda_q = \lambda_q(1 - k_{ep}), \tag{12}$$

$$\lambda_q^* = \lambda_q + \Delta\lambda_q, \tag{13}$$

$$\theta_0^* = \arctan(\frac{\lambda_q^*}{\lambda_q}), \tag{14}$$

$$\Phi_0^* = \sqrt{\lambda_q^{*2} + \lambda_d^2}. \tag{15}$$

6) CALCULATING Q-AXIS FLUX LINKAGE AND MOTOR PERFORMANCE

From the analysis result obtained in 4), the d-axis flux linkage is extracted. Finally, output torque property can be calculated by (16)–(18), where N_p, L_d, L_q, i_d, and i_q, represent the number of poles, d-axis inductance, q-axis inductance, d-axis

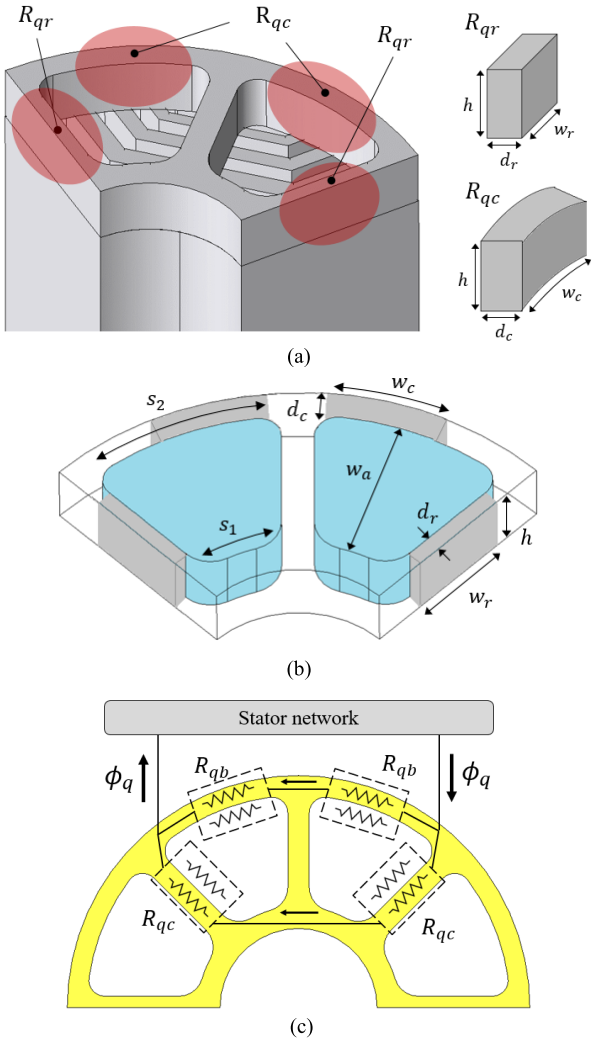

FIGURE 7. q-axis MEC conceptual diagrams of the end-plate: (a) reluctance of end-plate structure. (b) reluctance of air region. (c) q-axis MEC.

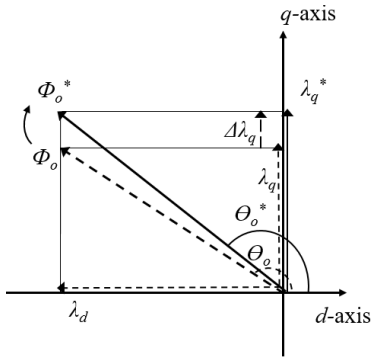

FIGURE 8. Phase diagram of the q-axis flux linkage.

current, and q-axis current, respectively.

$$L_q^* = \frac{\lambda_q^*}{I_q}, \tag{16}$$

$$L_d = \frac{\lambda_d}{I_d}, \tag{17}$$

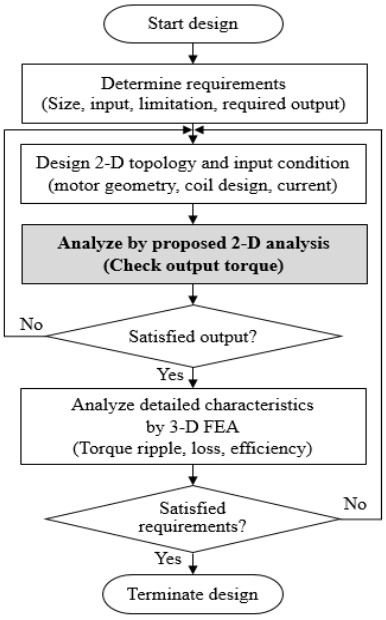

FIGURE 9. Application of the proposed method in the entire design process.

$$T = \frac{3}{2}\frac{N_p}{2}(L_d - L_q^*)i_d i_q. \tag{18}$$

D. APPLYING TO ENTIRE DESIGN PROCESS

Fig. 9 shows the application of the proposed method in the entire design process of the motor. The output power is the most important performance to be considered in the motor design. In particular, several design candidates need to be analyzed in the SynRM design process because the complicated geometry of air layers must be considered. From this perspective, the proposed method can partially replace the 3-D FEA, as shown in bold in Fig. 9.

Consequently, the iterative design process to obtain the designs, which satisfy the required output torque, can be realized 2-D based analysis. Hence, the design time can be significantly reduced.

III. RESULTS

To verify the proposed method, analyses with three different load conditions were performed and compared. The load conditions were set to 100%, 75%, and 50% of the rated current. In addition, to verify the applicability of the maximum torque per ampere control method, predominantly used when driving SynRM with maximum efficiency, the torque characteristics according to the current phase angle were analyzed. At each load condition, three different analyses were conducted: 1) 2-D FEA with neglecting the end-plate, 2) 3-D FEA, and 3) the proposed analysis method. The test bench for the experiment of SynRM is shown in Fig. 10.

Table 3 compares the results of the analyses. The 2-D FEA results show much higher torque performance at all analysis conditions since the end-plate effect was neglected. However, the results of 3-D FEA agree well with those of the proposed 2-D method, exhibiting differences of 2.0%, 5.0%, and

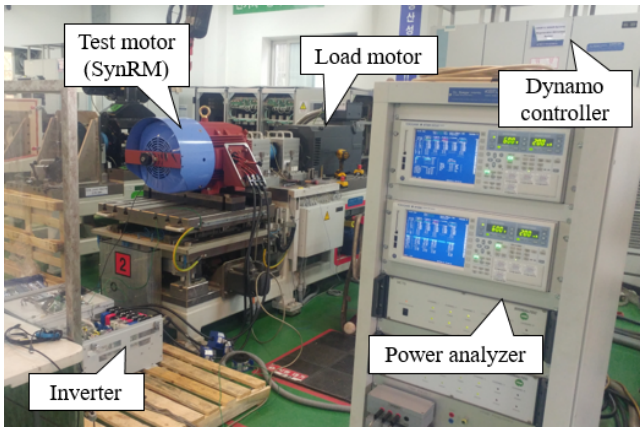

FIGURE 10. Test bench for the experiment.

TABLE 3. Analysis results at three different current conditions.

Contents		2-D FEA	3-D FEA	Proposed method
Rated Current (100%)	Current (A_{rms})	219.6	219.6	219.6
	Angle (deg)	73	73	73
	Torque (Nm)	452.4	398.9	406.1
75% current	Current (A_{rms})	164.8	164.8	164.8
	Angle (deg)	64	64	64
	Torque (Nm)	341.7	292.5	307.9
50% current	Current (A_{rms})	109.8	109.8	109.8
	Angle (deg)	60	60	60
	Torque (Nm)	205.3	174.1	186.1

TABLE 4. Analysis and test results at rated output power.

Contents	Test	3-D FEA	2-D FEA	Proposed method
Current (A)	219.6	219.6	187.6	215.5
Current angle (deg)	75	73	66	73
Torque (Nm)	398.3	398.9	398.1	398.5
Output power (kW)	75.1	75.2	75.1	75.1

6.5% at 100%, 75%, and 50% current conditions. Because the proposed method assumes the magnetic flux saturation, the higher accuracy appeared at the higher current conditions; some differences occur at low loads. However, a computational advantage of the proposed method is confirmed; this method completes the analysis in only a few minutes, unlike 3-D FEA, which consumed several hours.

Finally, the current and torque characteristics at the rated output of the target model were analyzed to compare the analyses with the test results, as summarized in Table 4. In conventional 2-D FEA, the required torque was obtained with the lowest current because the end-plate effect was not considered. In contrast, the results of 3-D FEA and the proposed method agree well with the experimental results, at the same output power with a difference of less than 1.9% with respect to current.

IV. CONCLUSION

This paper contributes to the rapid and effective design for the SynRM with an end-plate structure. The proposed analysis methodology was developed based on the q-axis MEC, 2-D FEA, and the flux linkage adjustment process. In addition, we present the entire design process using the proposed method. The method was validated by comparing analysis results with the 3-D FEA results for three different load conditions. Because the computational cost can be remarkably reduced, the proposed analysis method can be widely used as an effective design strategy for electric machines.

REFERENCES

[1] Y. Liang, H. Yu, and X. Bian, "Finite-element calculation of 3-D transient electromagnetic field in end region and eddy-current loss decrease in stator end clamping plate of large hydrogenerator," *IEEE Trans. Ind. Electron.*, vol. 62, no. 12, pp. 7331–7338, Dec. 2015.

[2] J. P. Lecointe, F. Morganti, F. Zidat, J. F. Brudny, R. Romary, T. Jacq, and F. Streiff, "Effects of external yoke and clamping-plates on AC motor external field," *IET Science, Meas. Technol.*, vol. 6, no. 5, pp. 350–356, Sep. 2012.

[3] J.-K. Lee, D.-H. Jung, K.-D. Lee, W. Jin, G. Lee, J. Lee, and Y. J. Oh, "A study on analysis of synchronous reluctance motor considering axial flux leakage through end plate," *IEEE Trans. Magn.*, vol. 55, no. 6, Jun. 2019, Art. no. 8201704.

[4] K.-C. Kim, D.-H. Koo, and J. Lee, "The study on the overhang coefficient for permanent magnet machine by experimental design method," *IEEE Trans. Magn.*, vol. 43, no. 6, pp. 2483–2485, Jun. 2007.

[5] R. Andreux, J. Fontchastagner, N. Takorabet, and N. Labbe, "A fast finite element model taking into account 3-D effects for the optimal design of micro-hybrid starters," *IEEE Trans. Magn.*, vol. 50, no. 5, May 2014, Art. no. 7400408.

[6] Y.-Y. Ko, J.-Y. Song, M.-K. Seo, W. Han, Y.-J. Kim, and S. Jung, "Analytical method for overhang effect of surface-mounted permanent-magnet motor using conformal mapping," *IEEE Trans. Magn.*, vol. 54, no. 11, Nov. 2018, Art. no. 8208005.

[7] H.-K. Yeo, D.-K. Lim, and H.-K. Jung, "Magnetic equivalent circuit model considering the overhang structure of an interior permanent-magnet machine," *IEEE Trans. Magn.*, vol. 55, no. 6, Jun. 2019, Art. no. 8201404.

[8] J.-G. Lee, R.-E. Kim, H.-K. Jung, and H.-K. Yeo, "Electromagnetic and thermal analyses of surface-mounted permanent magnet motor with flux-absorbing structure for enhancing overhang effect," *IET Electr. Power Appl.*, vol. 14, no. 11, pp. 2037–2043, Nov. 2020.

[9] A. Tessarolo, M. Mezzarobba, and R. Menis, "Modeling, analysis, and testing of a novel spoke-type interior permanent magnet motor with improved flux weakening capability," *IEEE Trans. Magn.*, vol. 51, no. 4, Apr. 2015, Art. no. 8103910.

[10] J.-Y. Song, J. H. Lee, Y.-J. Kim, and S.-Y. Jung, "Computational method of effective remanence flux density to consider PM overhang effect for spoke-type PM motor with 2-D analysis using magnetic energy," *IEEE Trans. Magn.*, vol. 52, no. 3, Mar. 2016, Art. no. 8200304.

[11] J.-H. Park, K.-T. Jung, Y.-H. Jung, M.-S. Lim, M.-H. Yoon, J.-P. Hong, and J.-W. Jung, "Design and verification for the torque improvement of a concentrated flux-type synchronous motor for automotive applications," *IEEE Trans. Ind. Appl.*, vol. 55, no. 4, pp. 3534–3543, Jul. 2019.

[12] P. Lazari, B. Sen, J. Wang, and X. Chen, "Accurate $d--q$ axis modeling of synchronous machines with skew accounting for saturation," *IEEE Trans. Magn.*, vol. 50, no. 11, Nov. 2014, Art. no. 8105704.

[13] X. Ge, Z. Q. Zhu, G. Kemp, D. Moule, and C. Williams, "Optimal step-skew methods for cogging torque reduction accounting for three-dimensional effect of interior permanent magnet machines," *IEEE Trans. Energy Convers.*, vol. 32, no. 1, pp. 222–232, Mar. 2017.

[14] K.-Y. Hwang, H. Lin, S.-H. Rhyu, and B.-I. Kwon, "A study on the novel coefficient modeling for a skewed permanent magnet and overhang structure for optimal design of brushless DC motor," *IEEE Trans. Magn.*, vol. 48, no. 5, pp. 1918–1923, May 2012.
[15] L. Wang, X. Bao, C. Di, and Y. Zhou, "Influence on vibration and noise of squirrel-cage induction machine with double skewed rotor for different slot combinations," *IEEE Trans. Magn.*, vol. 52, no. 7, Jul. 2016, Art. no. 8104404.
[16] O. Ocak and M. Aydin, "A new hybrid permanent magnet synchronous motor with two different rotor sections," *IEEE Trans. Magn.*, vol. 53, no. 11, Nov. 2017, Art. no. 8111705.
[17] J. Zhang, W. Chen, X. Huang, Y. Fang, J. Zhang, J. Ma, and W. Cao, "Evaluation of applying retaining shield rotor for high-speed interior permanent magnet motors," *IEEE Trans. Magn.*, vol. 51, no. 3, Mar. 2015, Art. no. 8100404.
[18] H.-W. Jun, J.-W. Lee, G.-H. Yoon, and J. Lee, "Optimal design of the PMSM retaining plate with 3-D barrier structure and eddy-current loss-reduction effect," *IEEE Trans. Ind. Electron.*, vol. 65, no. 2, pp. 1808–1818, Feb. 2018.
[19] E. Howard and M. J. Kamper, "Weighted factor multiobjective design optimization of a reluctance synchronous machine," *IEEE Trans. Ind. Appl.*, vol. 52, no. 3, pp. 2269–2279, May 2016.
[20] H.-C. Liu and J. Lee, "Optimum design of an IE4 line-start synchronous reluctance motor considering manufacturing process loss effect," *IEEE Trans. Ind. Electron.*, vol. 65, no. 4, pp. 3104–3114, Apr. 2018.
[21] J. Baek, M. M. Rahimian, and H. A. Toliyat, "Optimal design of PM assisted synchronous reluctance generators using lumped parameter model and differential evolution strategy," in *Proc. IEEE Energy Convers. Congr. Expo.*, Sep. 2009, pp. 2453–2459.
[22] H. Mahmoud, G. Bacco, M. Degano, N. Bianchi, and C. Gerada, "Synchronous reluctance motor iron losses: Considering machine nonlinearity at MTPA, FW, and MTPV operating conditions," *IEEE Trans. Energy Convers.*, vol. 33, no. 3, pp. 1402–1410, Sep. 2018.
[23] F. Cupertino, G. Pellegrino, and C. Gerada, "Design of synchronous reluctance motors with multiobjective optimization algorithms," *IEEE Trans. Ind. Appl.*, vol. 50, no. 6, pp. 3617–3627, Nov. 2014.

RAE-EUN KIM received the B.S. and M.S. degrees in electrical engineering from Seoul National University, Seoul, South Korea, in 2004 and 2009, respectively. From 2009 to 2011, he was a Research Engineer with the Research and Development Center, Hyundai Rotem Company, Uiwang, South Korea, where he worked on the development of traction motor of electric multiple units. From 2011 to 2015, he conducted research at the Electric and Elecrto System Research and Development Center, Hyundai Heavy Industries, Yongin, South Korea, where he worked on the development of motors for electric vehicles and industrial applications. He is currently working with the Korea Electronics Technology Institute, Bucheon, South Korea. His research interests include optimal design of electric machines and measurement of motor performance.

JAE-GIL LEE received the B.S. degree in electrical and electronic engineering from Pusan National University, Busan, South Korea, in 2013, and the Ph.D. degree from Seoul National University, Seoul, South Korea, in 2020. He is currently working with the Korea Electronics Technology Institute, Bucheon, South Korea, where he works on the development of actuators for robots and electric propulsion systems for vehicles and aircrafts. His research interest includes optimal design of electric machines.

JUNG-MOO SEO received the B.S. degree from the School of Electrical and Electronics Engineering, Chung-Ang University, Seoul, South Korea, in 2003, and the M.S. and Ph.D. degrees from the School of Electrical Engineering, Seoul National University, Seoul, in 2005 and 2016, respectively. He is currently with the Intelligent Mechatronics Research Center, Korea Electronics Technology Institute, Bucheon, South Korea, where he works on the development of electric machinery and actuators.

SEUNGYONG HAHN received the B.S., M.S., and Ph.D. degrees in electrical engineering from Seoul National University, Seoul, South Korea, in 1998, 2000, and 2003, respectively. From 2006 to 2015, he was a Research Engineer with the Francis Bitter Magnet Laboratory of MIT. From 2011 to 2015, he served with the Department of Mechanical Engineering, MIT. From 2015 to 2017, he was an Associate Professor with the Department of Mechanical Engineering, Florida State University, USA, and the National High Magnetic Field Laboratory, USA. From 2017 to 2019, he served as an Associate Professor with the Department of Electrical and Computer Engineering, Seoul National University, where he has been a Professor, since 2019. His research interests include large power and high field electric machines, superconducting and conventional, that cover electric power, renewable energy, biomedical, electric propulsion, and high energy physics applications.